University of Baghdad
College of Engineering
JOURNAL OF ENGINEERING

Journal of Engineering

journal homepage: www.jcoeng.edu.iq
Number 4 Volume 24 April 2018

Mechanical and Energy Engineering

Effect of Using Extra Fins on the Pin Fin Classic Geometry for Enhancement Heat Sink Performance using EGM Method

Kadhum Audaa Jehhef
Instructor
Department of Equipment and Machine
Institute of Technology, Middle Technical University
Email: kadhum.audaa@yahoo.com

ABSTRACT

In the present study, the effect of new cross-section fin geometries on overall thermal/fluid performance had been investigated. The cross-section included the base original geometry of (triangular, square, circular, and elliptical pin fins) by adding exterior extra fins along the sides of the origin fins. The present extra fins include rectangular extra fin of 2 mm (height) and 4 mm (width) and triangular extra fin of 2 mm (base) 4 mm (height). The use of entropy generation minimization method (EGM) allows the combined effect of thermal resistance and pressure drop to be assessed through the simultaneous interaction with the heat sink. A general dimensionless expression for the entropy generation rate is obtained by considering a control volume around the pin fin including a base plate and applying the conservations equations of mass and energy with the entropy balance. The dimensionless numbers used includes the aspect ratio (ε), Reynolds number (Re), Nusselt number (Nu), and the drag coefficients (C_D). Fourteen different cross-section fin geometries are examined for the heat transfer, fluid friction, and the minimum entropy generation rate. The results showed that the Nusselt number increases with increasing the Reynolds number for all employed models. The ellipse models (ET and ER-models) give the highest value in the Nusselt number as compared with the classical pin fins. The fin of the square geometry with four rectangular extra fins (SR-models) gives an agreement in Nusselt number as compared with the previous study.
Keywords: Pin Fin, Heat Sink, EGM method.

تأثير استخدام زوائد زعنفية مع الشكل التقليدي للزعانف الابرية على تعزيز الاداء الحراري للزعانف باستخدام طريقة تقليل التولد الانتروبي

د. كاظم عودة جحف
قسم المكائن والمعدات
معهد تكنولوجيا- بغداد, الجامعة التقنية الوسطى

الخلاصة

في البحث الحالي تم دراسة تاثير استخدام مقطع لشكل زعنفة جديد لتحسين المقطع العرضي للزعانف الابرية التقليدية على الخواص الحرارية الكلية والجريان للمائع، والمقاطع العرضية السابقة للزعانف كانت على شكل (مثلث، مربع، دائرة او بيضوي) حيث تم في هذا البحث اضافة زوائد اضافية للشكل الاصلي للزعنفة تتضمن زائدة بشكل مستطيل بعرض 4 ملم وارتفاع 2 ملم او زائدة بشكل مثلث بطول قاعدة 4 ملم وارتفاع 2 ملم، وتبين ان استخدام طريقة تخفيض توليد الانتروبي (EGM) تسمح بتركيب
https://doi.org/10.31026/j.eng.2018.04.01

تاثير كل من المقاومة الحرارية وانخفاض الضغط والتي يتم تحديدها من خلال محاكاة التداخل في التاثير مع الزعانف. والتعبير اللابعدي العام لمعدل توليد الانتروبي يتحصل من خلال فرض حجم محدد حول الزعنفة الابرية المدروسة وتطبيق معادلة حفظ الطاقة والكتلة مع موازنة الانتروبي. المقادير اللابعدية المستخدمة هي نسبة الشكل (ε) ، عدد رينولدز (Re)، عدد نسلت (Nu) ومعامل الاعاقة (C_D) . وتم دراسة اربعة عشر شكلا هندسيا مختلفا للزعانف لتحصيل النتائج الخاصة بكل من انتقال الحرارة واحتكاك المائع ونسبة تقليل توليد الانتروبي. واوضحت النتائج النظرية ان عدد نسلت يزداد مع زيادة عدد رينولدز ولجميع النماذج المدروسة. وعندما نستخدم الشكل البيضوي مع زوائد مستطيلة ومثلثة نحصل على اعلى نسبة زيادة لقيمة عدد نسلت مقارنة مع الزعانف الابرية التقليدية. استخدام النموذج الهندسي الجديد وهو شكل مربع مع اربع زوائد خارجية مستطيلة يعطي نسبة تطابق جيدة مقارنة مع البحوث السابقة

الكلمات المفتاحية: الزعانف الابرية, سحب الحرارة, طريقة EGM .

1. INTRODUCTION

These techniques can be considered as passive techniques because generally use surface or geometrical modifications. These heat transfer enhancement techniques have many practical applications for internal cooling of turbine airfoils, combustion chamber liners and electronics cooling devices, biomedical devices, and heat exchangers. Entropy, the thermodynamic measure, is an analytic tool that may serve to evaluate phenomena that dominate our lives and therefore belongs to the realm of philosophy. Since the trends show a universal trend for equalization, like the concepts of codification and globalization, an increase in global entropy is appearing as an obvious result**, Shaukatullah, et al., 1996,** and **George, 1995**. Thus, what is the entropy? Entropy has been defined as the residual irreversible energy generated in thermodynamics **Boltzmann, 1872.**

The optimistic design of thermal systems can be achieved by minimizing entropy generation in the systems. This issue has been the topic of great importance in many engineering fields such as heat exchangers, cooling of nuclear reactors, MHD power generators, geophysical fluid dynamics, energy storage systems, cooling of electronic devices, etc. Entropy generation is associated with many processes such as heat transfer across finite temperature gradient, characteristics of convective heat transfer, magnetic field effect, viscous dissipation effect etc. Pin-fin heat sinks have an advantage of impeding the development of the thermal boundary layer in a unidirectional flow at the expense of an increase in pressure drop **Khan,** and **Culham, 2003** and **Khan, et al., 2006**. There are many cross-section geometries of the fins different in the thermal and flow performance, well; the main question here is which type of heat sink performs better? So far, several researchers have been interested in this question and sought proper answers to it. **Hossain, 2006** presented the simultaneous optimization of heat sink design parameters based on a minimization of the entropy generation associated with thermal resistance and fluid pressure drop. All relevant design parameters such as geometric parameters of a heat sink, source and bypass configurations, heat dissipation, material properties and flow conditions can be simultaneously optimized to characterize a heat sink that minimizes entropy generation and in turn results in a minimum operating temperature of an electronic component. The results showed thermally optimized heat sink showed better thermal performance than the optimized heat sink obtained from entropy generation minimization but with higher entropy generation rate and pressure drop penalty. **Khan, et al., 2007** presented a study to examine the effect on overall thermal/fluid performance associated with different fin geometries, including, rectangular plates as well as square, circular and elliptical pin fins. And their results clearly indicated that the preferred fin profile is very dependent on these parameters. **Kim, et al., 2008** gave a comparison between the thermal performances of the two types of heat sinks most commonly used in the electronic equipment cooling: plate- equipment cooling: plate-fin and pin-fin heat sinks. In order to obtain the fluid flow and thermal characteristics of heat sinks, an experimental investigation was conducted. The results showed a contour map, which depicts the ratio of the

thermal resistances of the optimized plate-fin and pin-fin heat sinks as a function of dimensionless pumping power and dimensionless length. The contour map indicated that optimized plate-fin heat sinks possessed lower thermal resistances than optimized pin-fin heat sinks when dimensionless pumping power is small and the dimensionless length of heat sinks is large. On the contrary, the optimized pin-fin heat sinks have smaller thermal resistances when dimensionless pumping power is large and the dimensionless length of heat sinks is small. **Khan, 2010** employed an entropy generation minimization procedure to optimize the overall performance (thermal and hydrodynamic) of isolated fin geometries and pin-fin heat sinks. The formulation for the dimensionless entropy generation rate was obtained in terms of fin geometry, Prandtl numbers ≥ 0.71 from single pins (circular and elliptical) with and without blockage as well as pin-fin arrays (in-line and staggered). **Carlos, et al., 2013** gave a comparison of the performances of online and offset micro pin-fin heat sinks with variable fin density. They used water as a coolant in the single phase and laminar regime. 4748 micro flat fins with rounded sides, which are distributed in three different sections along the flow length, are used in these configurations. Their results indicate that the offset micro pin-fin heat sink is a good alternative for cooling the IC chips of 2016. **Naoko, et al., 2014** presented experimental and numerical investigation of heat sinks with miniature/micro pins and the effect of the pin size, pin height and the number of pins on heat transfer characteristics of heat sinks. Five types of basic heat sink models are investigated. The whole heat transfer area of heat sinks having the different pin size, pin height and the number of pins respectively is kept constant. They showed that the heat sink temperature rises with increase in the number of pins.

That is, the heat sink with miniaturized fine pins showed almost no effect on the heat transfer enhancement. **Huashuai, et al., 2015** developed a finite element analysis for determining heat transfer from in-line and staggered-pin fin heat sinks used in electronic packaging applications. They used this method to predict the heat transfer performance of the new heat sink with woven fabric structure, called fabric pin fin heat sink. Their results show that the minimum temperature of heat sink decreases with an increase of pin fin length, but the decreasing amplitude has decreased. **Pakrouh, et al., 2015** presented a numerical investigation in which thermal performance characteristics of pin fin heat sinks enhanced with phase-change materials (PCMs) designed for cooling of electronic devices are studied. The paraffin RT44 HC is poured into the aluminum pin fin heat sink container. They showed that increasing the number, thickness, and height of fins leads to a significant decrease in the base temperature as well as the operating time of the heat sink. **Therisa, et. al., 2016** presented a modification of classical heat sink depends on various geometric parameters like, fin length, fin height, fin thickness, number of fins, base plate thickness, space between fins, fin shape or material etc. and based on the concept of standard pin fin, splayed pin fin and hybrid pin-fin heat sinks. They observed that the pyramid structure gives a result of increasing heat dissipation rate, but splayed pin fins given more heat transfer beyond this hybrid heat sink performed well.

Chougule, et al., 2016 studied the effects of design parameters and the optimum design parameters for a Pin-Fin heat sink (PFHS) under multi-jet impingement case with thermal performance characteristics have been investigated by using Taguchi methodology. They showed that the analysis of the Taguchi method reveals that, all the parameters mentioned have equal contributions in the performance of heat sink efficiency. Finally, the present study focused on the enchantment the cross-section of the pin cylindrical fin. From the previous research revision, it may be noted that there exists a large amount research work on the performance of classic cross-section geometry of pin-fins. Therefore, the main aim of this study is concerned with the new or developed other geometric modeled by entropy generation minimization.

2. HEAT SINK MODELS

Regard an original pin fin of arbitrary cross section (triangular, square, circular, or elliptical) with an extra two or four triangular or square, fins geometry of a heat sink as shown in **Table.1**. The dimensions of the base plate are ($L_b \times W_b \times t_b$). Each pin fin has different geometry. The approach velocity of the air is (U_{app}). The direction of the flow is parallel to the x-axis. The bottom surface is kept at constant temperature (T_b) and the top surface is insulated. The average wall temperature of the pin surface is (T_f). The ambient temperature and the tube wall temperatures are fixed at 300 and 365 K, respectively. The heat source is idealized as a constant heat flux (Q) boundary condition at the bottom surface of the base plate. The mean temperature of the heat source is (T_s). It is assumed that the heat sink is fully shrouded and the heat source is situated at the center of the base plate. It was assumed that the fluid temperature is averaged over the height of the heat sink, so the fluid temperature (T_a) is the bulk mean fluid temperature. Fully developed heat and fluid flow are assumed in the analysis, and the thermophysical properties are taken to be temperature independent. In designing a heat sink, the size and the heat load are the usual constraints.

2.1 Model Development and Fanatical Solution

Regard an original pin fin of arbitrary cross-section as shown in **Fig.1**, which is extended from a base plate. The approach velocity of the air is (U_{app}) and the ambient temperature of the air is assumed to be (T_a). The surface temperature of the pin fin wall is (T_f) > (T_a). This study assumes the following design considerations, **Khan,** and **Culham, 2003:**

a. Each pin is of uniform diameter, D, and height, H, with the circular cross-section.
b. The pins are uniformly spaced on the base plate.
c. The fin tips are adiabatic.
d. There is no air flow bypass, i.e. the heat sink is fully ducted.
e. The air flow is normal to the pin-axis.
f. The approach velocity is uniform for each row in a heat sink.

2.2 Performance of Heat Sinks

2.2.1 Heat Sink Resistance

The thermal performance of a pin-fin heat sink depends upon the total thermal resistance of the system consists of a heat source on one side of the base plate and a cooling medium on the other side. A Control volume is defined in **Fig. 1** to calculate thermal resistance in a single circular pin **Khan** and **Culham, 2003**. Assuming that the thermal spreading and contact resistances are negligible, the total thermal resistance (R_{tot}) can be written as:

$$R_{tot} = \frac{1}{\frac{1}{R_f} + \frac{1}{R_b}} \quad (1)$$

where

$$R_f = \frac{1}{\sqrt{h_f P k_{fin} A_c}\,\tanh(mH)} \quad (2)$$

$$R_b = \frac{1}{h_b (LW - A_f)} \quad (3)$$

With the fin parameter

$$m = \sqrt{\frac{Ph_f}{k_{fin}A_f}} \quad (4)$$

The average heat transfer coefficient of the fin:

$$h_f = \frac{Nu_f k_{film}}{L_f} \quad (5)$$

The average heat transfer coefficient of the base plate:

$$h_b = \frac{Nu_b k_{film}}{L_b} \quad (6)$$

where the dimensionless average heat transfer coefficients Nu_f for the selected geometries **Culham et. al., 2007**:

$$Nu_f = C_1 \mathrm{Re}_f^{1/2} \mathrm{Pr}^{1/3} \quad (7)$$

where C_1 is a constant which depends upon the longitudinal and transverse pitches, the arrangement of the pins, and thermal boundary conditions. For isothermal boundary condition, for an in-line arrangement it is given by **Culham, et al., 2007**:

$$C_1 = \frac{[0.2 + \exp(-0.55S_T)]S_T{}^{0.785}S_L{}^{0.212}}{(ST - 1)^{0.5}} \quad (8)$$

and Nu_b for the base plate can be written as **Culham, et al., 2007**:

$$Nu_b = 0.75 \mathrm{Re}_b^{1/2} \mathrm{Pr}^{1/3} \quad (9)$$

The fin Reynolds number can be defined as:

$$\mathrm{Re}_f = \frac{U_{app}L_f}{\nu} \quad (10)$$

The base plate Reynolds number can be defined as:

$$\mathrm{Re}_b = \frac{U_{app}L_b}{\nu} \quad (11)$$

Thermal spreading resistance occurs when the heat spreads from a surface-mounted heat source into a conducting solid (base plate, in the case of a heat sink) a planar rectangular heat source situated on the bottom surface of the base plate having a thickness (t_b) and thermal conductivity (k_{fin}). The base plate is cooled along the top surface through a uniform film coefficient.

2.2.2 Entropy generation minimization (EGM) technique

If the base temperature of the heat sink (T_b) is averaged and assumed to be constant, the energy balance for the control volume **Fig.1**, **Kim, et al., 2008** is as the following:

The mass rate balance for the CV gives:

$$\frac{dm_{cv}}{dt} = \dot{m}_{in} - \dot{m}_{out} \quad (12)$$

For steady state, it reduces to:

$$\dot{m} = \dot{m}_{in} = \dot{m}_{out}$$

The energy rate balance can be written as:

$$\frac{dE_{cv}}{dt} = Q - \dot{W}_{cv} + \dot{m}_{in}(e_{in} + P_{in}u_{in}) - (\dot{m}_{out}u_{out} + P_{out}u_{out})$$

Thus the energy rate balance reduces to:

$$Q = \dot{m}[(u_{out} + P_{out}u_{out}) - (u_{in} + P_{in}u_{in})] \quad (13)$$

The combination of specific internal and flow energies is defined as specific enthalpy; therefore, the energy rate balance reduces further to:

$$Q = \dot{m}(h_{out} - h_{in}) \quad (14)$$

From the second law of thermodynamics **Kim, et al., 2008**:

$$\frac{dS_{CV}}{dt} = \dot{m}(S_{in} - S_{out}) + \frac{Q}{T_a} + \dot{S}_{gen} \quad (15)$$

For steady state, $dScv/dt$=0, and the total heat transferred from the baseplate $Q=Q_f+Q_b$, so the entropy rate balance reduces to, **Kim, et al., 2008:**

$$\dot{S}_{gen} = \dot{m}(S_{out} - S_{in}) - \frac{Q}{T_a} \quad (16)$$

From a force balance, the total drag force can be written as **Kim, et al., 2008**:

$$F_D = -(P_{out} - P_{in})A_p \quad (17)$$

The mass flow rate is given by:

$$\dot{m} = \rho A_p U_{app} \quad (18)$$

The enthalpy difference in Eq. (13) can be written in terms of entropy and pressure differences using Gibb's equation [$dh=Tds+(1/\rho)dP$] **Kim, et al., 2008**:

$$(h_{out} - h_{in}) = T_a(S_{out} - S_{in}) + \frac{1}{\rho}(P_{out} - P_{in}) \quad (19)$$

Consider a fin of the arbitrary constant cross-section, which is immersed in a uniform stream of air with velocity U_{app} and ambient temperature (T_a). The fin is assumed to be isothermal at a temperature (T_f) as shown in **Fig.2**. **Bejan, 1996** Combines Eqs. (12-19) to obtain the entropy generation rate written as:

$$\dot{S}_{gen} = \frac{Q^2 R_{tot}}{T_a T_b} + \frac{F_D U_{app}}{T_a} \quad (20)$$

Whereas, the drag force for the fin of the arbitrary cross-section can be written as:

$$F_D = C_D\left[\frac{1}{2}\rho U_{app}^2\right]A_p \quad (21)$$

The total drag coefficient C_D can be given as the sum of both drag coefficients.

$$C_D = \frac{C_2}{\sqrt{\mathrm{Re}_f}} + C_3 + \frac{C_4}{\sqrt{\mathrm{Re}_f}} \quad (22)$$

Where (C_2=5.784, C_3=1.152, and C_4=1.260) are the constants depending upon the geometry. For isothermal boundary conditions, the dimensionless entropy generation rate can be defined as:

$$N_s = \frac{\dot{S}_{gen}}{\left(Q^2 U_{app} / k_{film} \nu T_a^2\right)} = N_{sh} + N_{sf} \quad (23)$$

$$N_{sf} = \frac{1}{2} C_D B_\gamma \mathrm{Re}_f^2 \, \varepsilon \quad (24)$$

Finally, by using the Eqs. (1-11) with Eq. (24) to obtain the dimensionless form of the entropy generation rate for any arbitrary cross section is written as, **Khan** and **Culham, 2006**:

$$N_s = \frac{\dot{S}_{gen}}{\left(Q^2 U_{app} / k_f \nu T_a^{\,2}\right)} = \frac{(T_a/T_b)k_{eq}}{\mathrm{Re}_f}\left[\frac{1}{\sqrt{C_5 Nu_{Lc} k_{eq}}.\tanh(\gamma_{Lc}\sqrt{C_6 Nu_{Lc} k_{eq}}) + C_7 Nu_{Lc} k_{eq}}\right] + \frac{1}{2} C_D B_\gamma \mathrm{Re}_f^2\, \gamma_{Lc}$$

(25)

Where $B_\gamma = \rho \nu^3 k T_a / Q^2$ is a fixed dimensionless duty parameter accounts for the importance of fluid friction irreversibility relative to heat transfer irreversibility? The duty parameter B_γ is fixed as soon as the fluid, fin material, and the base heat transfer rate is specified. The greater the base heat transfer rate, the smaller will be the fluid friction irreversibility. The constants C_5, C_6, and C_7 in Eq. (24) depend on the geometry of the fin and are given by:

$$C_5 = \frac{PA_f}{L_f^{\,3}} \quad , C_7 = \frac{W_b}{L_b} - \frac{A_b}{L_b^2} \quad \text{and} \quad C_6 = \frac{PL_f}{A_f}$$

2.2.3 Overall Heat Transfer Coefficient for Heat Sink

$$Q = Q_b + Q_f \qquad (26)$$

Where

$$Q_b = (hA)_b Q_b$$

$$Q_f = (h\eta A)_f\, Q_b$$

where $A_b = L_b W_b - A_f$, and (A_f) depends on the geometry of the cross-section of the fin illustrated in **Table.1**. The efficiency of the fin η_f with constant convective heat transfer coefficient and an insulated tip is

$$\eta_f = \frac{\tanh(mH)}{mH} \qquad (27)$$

As shown in **Fig.2**, the present model using a single fin with a height of (H=25.26 mm) and a rectangular base plate with dimensions of (L_b=62.69 mm) and (W=58.42 mm) and thickness of (t_b=2.24 mm). Each pin fin is in the shape of an ellipse with a major axis of (b_1=15.54 mm) and a minor axis of (a_1=10.27 mm), equilateral triangle with a side length of (h=10.54 mm) and rectangular with dimensions of (a=15.54 mm) and (b=10.27 mm), square of (a=10.27 mm) side and finally use a circle shape of diameter of (d=10.27 mm). The present extra fins includes rectangular extra fin of (t=2 mm) (height) and (b=4 mm) (width) and triangular extra fin of (b=2 mm) (base) (h=4 mm) (height). Finally, the required equations solved by MATLAB code and the solution procedure employed in this study presented in **Fig.3.**

3. RESULTS AND DISCUSSIONS

The objective of this study is to determine an optimal fin geometry by minimizing the dimensionless entropy generation rate for different design variables including (Ac cross-sectional area), (Ap plan form area for drag force), (P fins perimeter), (Lc fins characteristic length) and (U_{app} apparatus velocity) and (Re Reynolds number). In each case, the optimum approach velocity/Reynolds number is determined to correspond to the minimum entropy generation rate. The problem is solved for three different longitudinal and transverse pitch ratios and the overall performance is compared to all fins geometry.

The influences of the axis ratio (ε) and the using of two rectangular and triangular extra fins along the sides of the original geometry on the drag force for all models of cross-sections fins are shown in **Fig. 4** Clearly, (TR-model) the triangular fin with two square extra fins cross section is the worst choice, due to the highest drag force which is about (0.0043 N) and the model of (CT-model)

circular fin with triangular extra fins cross section is the best choice for the lowest drag force which is about (0.0021 N). The drag force for the elliptical geometry decreased monotonically from (0.0034 N) at (ε= 1) to the (0.00012 N) at (ε=0) due to the streamlined geometry of the elliptical model (ET-model) as compared with the other models.

Fig. 5 Illustrates the effect of the axis ratio (ε) on the Nusselt number for all models of cross-sections fins the results show that the heat transfer rate of (ER-model) elliptical fin with rectangular extra fin give the maximum values of the Nusselt number and decreases from (18.9) at (ε= 1) to (27.2) at (ε= 0.4) and then becomes constant with the same profile with (ET-model) but with little deference and the other models give construct profile which show increased the Nusselt number with increasing axis ratio (ε). **Fig.6** shows the effects of the Reynolds number based on the characteristic length of the fin on the Nusselt number for all models of cross-section fins. The results indicates that the Nusselt number increased as increases the Reynolds number increasing for all models but the (ER-model) and (ET- model) recorded an increase to maximum value which is about (Nu= 31.255) at ($Re=1.7\times10^3$) and then decreasing as the Reynolds number increases while the anther models increases as the Reynolds number is increased due to increasing the heat transfer rate as increasing the Reynolds number.

Figs.7 show the effect of the Reynolds number based on the characteristic length of the fin on the dimensionless entropy generation rates (Ns) Eq. (25) for all models of cross-sections fins. The results show that as expected fin geometries have constant Ns, but, for (ER- model) elliptical geometry, it decreases from (Ns 1.2) at Re = 0 (SS- model) to (Ns =0.05) at ($Re = 2.5\times10^3$) (ET-model) due to this geometry will vary the direction of the fluid flow. Where the maximum (Ns) exists at (1.52) for (CT-model). Using the model which have four extra fins on the sides caused to obtain an increase in the Nu about 10% compared with the model with two extra fins (ES- model) elliptical geometry.

The effect of Reynolds number on the dimensionless entropy generation rates for all models of cross-sections fins had been plotted in the **Figs. 8**. The results show that the entropy generation rates (S_{gen}) decrease with increasing Reynolds number for all models, and the TT-model triangular fin with triangular extra fins (TT- model) appeared high value of entropy generation rates. The use of four extra fins decreases the dimensionless entropy generation rates about (6 %) percent, due to this geometry increased the fluctuating fluid near the fin surface.

The dimensionless total entropy generation rate, Ns, includes the contributions due to heat transfer and viscous friction. As the approach velocity increased, the contribution due to heat transfer, (N_{sh}), decreased and that of viscous friction, (N_{sf}), increased for each of the geometries considered. This behavior is shown in **Figs. 9** for the (SR and TR-models). An optimal approach velocity (U_{app}) results away from which the dimensionless total entropy generation rate would increase. The optimal (Uapp) exists for all geometries depending upon the wetted surface area, where the (SR-models) give a higher value of dimensionless entropy generation Rates (Ns) than (TR-models). But the (TR-models) give a higher value of (Nsf) and (Nsh) than (SR-models).

Fig.10 illustrates the effect of the approach velocity for the (CR and SR-models) circular and square fin geometry with two rectangular extra fins. The (CR models) gave a higher value than (SR-models) of dimensionless entropy generation Rates (Ns). And the (CR-models) gave a higher value of (Nsf) and (Nsh) than (SR-models). **Fig.11** shows the effect of fin perimeter (P) on the dimensionless entropy generation rates for all models of fin geometry with rectangular extra fins for the axis ratio (ε= 0 to 1). The figure shows that the dimensionless entropy generation rates (S_{gen}) decreased with the increases the fin perimeter (P).

A Comparison of the present analytical results with previous studies is plotted in **Fig. 12.** The figure

shows that the enhancement of adding rectangular and triangular extra fins along the sides of triangular and square of the (TR and SR-models) with the original geometry was studied by (**Khan et al., 2006**) for square, circular, ellipse and rectangular geometries. The fin square geometry with rectangular extra fins (SR-models) shows an agreement in Nussselt number of (11.8 %) compared with the high value of rectangular plate (RFP- Khan model). The results show that the improvement of using the rectangular and triangular extra fins along the sides of the ellipse fins (ET and ER-models) with the original geometry studied by **Khan, 2010** for square, circular, ellipse and rectangular geometries. The ellipse model (ET and ER-models) presented highest values in this study and with increases in the Nusselt number about (25.21%) when compared with the (EPF-Khan model). Nevertheless, it increased with the increase of the ReLc until it reached the value of (Nu=31.42) at (Re=1500) and then it decreased as the Re increase until reaching the value of (Nu=21.12) at (Re = 2535).

4. CONCLUSIONS

New suggested arbitrary fin geometries having the same wetted surface area are compared according to the heat transfer, drag force, and dimensionless total entropy generation rate. The (TT and TR-models) geometries were found to be the worst choice from the point of view of heat transfer and drag force and hence from the point of view of total entropy generation rate. Whereas, the (CT-model) geometry appeared to be as the best from the point of view of drag force. For the square and triangular fins, geometry with rectangular extra fins (SR and TR-models) appeared to be as the best from the point of view of the dimensionless total entropy generation rate for low approach velocities and small wetted surface areas. The elliptical geometry is the next favorable geometry from the point of view of total entropy generation rate for higher approach velocities and with low axis ratios. It offers higher heat transfer coefficients and lower drag force as the axis ratio is decreased and the approach velocity is increased. The results showed that the fin of a square with rectangular extra fin (SR-models) geometry shows an agreement in Nusselt number as compared with that of the previous study. The lowest Nusselt number value of the studied models was found for the triangular fin with triangular extra fin (TT -model). But the ellipse models (ET and ER-models) give the highest value in the study when compared with the same data of other research.

REFERENCES

- Bejan, A., 1996, Entropy Generation Minimization, CRC Press, New York.
- Boltzmann L., 1872, Further studies on the thermal equilibrium between gas molecules, Wien Ber., 66, pp-275.
- Carlos A. Rubio-Jimenez, Satish G. Kandlikar, and Abel Hernandez-Guerrero, 2013 Performance of Online and Offset Micro Pin-Fin Heat Sinks With Variable Fin Density, IEEE Transactions on Components, Packaging and Manufacturing Technology, vol. 3, no.1.
- Chougule, N. K., Parishwad G. V., 2016, Optimization of Pin Fin Heat Sink Using Taguchi Method, World Academy of Science, Engineering and Technology International Journal of Mechanical and Mechatronics Engineering Vol:3, No:4.
- Culham, J.; Khan, W.A.; Yovanovich, M.; Muzychka, Y., 2007, The Influence of Material Properties and Spreading Resistance in the Thermal Design of Plate Fin Heat Sinks. J. Electron. Package, 129, 76–81.
- George N. Saridis, 1995, Entropy as a Philosophy, PhD theses, La Fin des Certitudes Editions Odile Jacob, Paris France.

- Hossain M. R., 2006, Optimization of Heat Sinks with Flow Bypass Using Entropy Generation Minimization, Master of Applied Science in Mechanical Engineering Waterloo, Ontario, Canada.
- Huashuai Zhang, Jiyong Hu, Xudong Yang, Yuling Li, 2015, Evaluation on Heat Transferring Performance of Fabric Heat Sink by Finite Element Modeling, Journal of Textile Science and Technology, 1, 25-32.
- Khan W. A. and Culham J. R., 2003, The Role of Fin Geometry in Heat Sink Performance, Proceedings of IPACK03 International Electronic Packaging Technical Conference and Exhibition July 6-11, Maui, Hawaii, USA.
- Khan W. A., 2010, Modeling of Fluid Flow and Heat Transfer for Optimization of Pin-Fin Heat Sinks, Ph.D. thesis, University of Waterloo, Mechanical Engineering, Waterloo, Ontario, Canada.
- Khan W. A., Culham, J. R., Yovanovich, M. M., 2007, Optimal Design of Tube Banks in Cross flow Using Entropy Generation Minimization Method, Journal of Thermo Physics and Heat Transfer Vol. 21, No. 2, pp372-379, April–June.
- Khan W. A., Culham J. R., Yovanovich M. M., 2006, The Role of Fin Geometry in Heat Sink Performance, Transactions of the ASME Vol. 128, pp 324-330.
- Kim S. J., Kwon, D., Hee, H., 2008, Comparison of Fluid Flow and Thermal Characteristics of Plate-Fin and Pin-Fin Heat Sinks Subject to a Parallel Flow, Department of Mechanical Engineering.
- Naoko Matsumoto, Toshio T., 2014, Yasushi K., Heat Transfer Characteristics of Square Micro Pin Fins under Natural Convection, Journal of Electronics Cooling and Thermal Control, 4, 59-69.
- Pakrouh, R., M. J. Hosseini, and A. A. Ranjbar, 2015, A parametric investigation of a PCM-based pin fin heat sink, Mech. Sci., 6, 65–73.
- Shaukatullah, H., Storr, W. R., Hansen, B. J., Gaynes, M. A.,1996, Design and Optimization of Pin Fin Heat Sinks for Low-Velocity Applications, Proc. Int. Electronics Packaging Conference, pp. 486–494.
- Therisa, T., Amarnathvarma A., Dipesh T., 2016, CFD Analysis of Various Height of Pin Fin Heat Sink in Inline Arrangement, Volume 1 Issue 1, 1, 1-6.

NOMENCLATURES

B_γ	duty parameter
C1 to C4	equation constants
C4 to C7	geometry constants
C_D	total drag coefficient
F_D	total drag force, N
$h_{f,}\ h_b$	base plate and fin average heat transfer coefficient, W/m^2K
k_{eq}	ratio of thermal conductivity of fluid to the fin material, W/mK
k_{film}	air film thermal conductivity, W/mK
k_{fin}	fin material thermal conductivity, W/mK
$L_{b,}\ L_f$	base plate and fin characteristic length in flow direction, m
m	fin performance parameter, m^{-1}
m_{in}, m_{out}	air mass flow rate in the inlet and outlet, kg/sec
N_s	total dimensionless total entropy generation rate
N_{sf}	fluid flow irreversibility

N_{sh}	heat transfer irreversibility
Nu_b, Nu_f	base plate and fin Nusselt number.
P_{in}, P_{out}	pressure in the inlet and outlet, W/K
Pr	Prandtl number
Q	total base plate heat flow rate, W
Q_b, Q_f	base plate and fin heat flow rate, W
R_b, R_f	base plate and fin overall resistance of a fin, K/W
Re_b, Re_f	base plate, and fin Reynolds number.
R_{tot}	total thermal resistance, K/W
S_{gen}	total entropy generation rate, W/K
S_{in}, S_{out}	entropy generation rate in the inlet and outlet, W/K
T_a	air film temperature, K
T_b	base plate bottom surface temperature, K
T_f	pin fin surface wall surface temperature, K
T_s	mean temperature of the heat source is, K
U_{app}	approach velocity of the fluid, m/s

Geometrical Symbols

a	length side of the square fin, m
a_1,b_1	semi-major and minor axes of the elliptical fin, m
A_f	crosses sectional area of the fin, m^2
A_p	free stream cross-sectional area, m^2
b	width of rectangular extra fin, m
d	circular pin fin diameter, m
h	length of triangular sides fin, m
H	fin height, m
h_1	height of triangular sides fin, m
L_b	base plate length in the downstream direction, m
P	perimeter of the fin, m
S	side of a square fin, m
S_L	pin spacing in streamwise direction, m
S_T	pin spacing in spanwise direction, m
t_b	base plate thickness, m
W_b	base plate width, m

Greek Symbols

ε	ratio of the plate sides= t_b/L
ν	kinematic viscosity of fluid film, m^2/s
ρ `	fluid density, kg/m^3
γ_{Lc}	aspect ratio, H/L.
η_f	fin efficiency.

Subscripts

b	base plate
f	pin fin
in	inlet
out	outlet

Fin Geometry Symbols

TT	triangular fin with triangular extra fin

TR	triangular fin with rectangular extra fin
ST	square fin with triangular extra fin
SR	square fin with rectangular extra fin
CT	circular fin with triangular extra fin
CR	circular fin with rectangular extra fin
ET	ellipse fin with triangular extra fin
ER	ellipse fin with rectangular extra fin
RPF	rectangular plate fin of the previous work.

Table 1. Fin cross-section geometries with rectangular and triangular extra fins.

Fin cross-section geometry with Rectangular extra fins	Area, Perimeter and Characteristic Length	Fin cross-section geometry with Triangular extra fins	Area, Perimeter and Characteristic Length
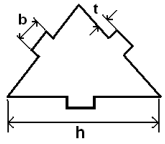	TR-Model $Ac = (hh_1) + 3(bt)$ $Ap = hH$ $P = 3(h - b) + 6t + 3b$ $Lc = h1$	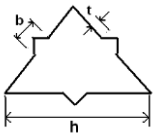	TT-Model $Ac = 0.5(hh_1) + 3(0.5bt)$ $Ap = hH$ $P = 3(h - b) + 6\sqrt{(t + 3b)}$ $Lc = h1$
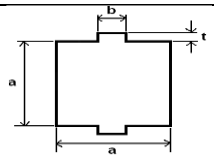	SR-Model $Ac = a^2 + 2(bt)$ $Ap = aH$ $P = 4a + 4t$ $Lc = a+2t$	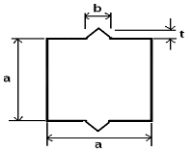	ST-Model $Ac = a^2 + 2(0.5bt)$ $Ap = aH$ $P = 4a+ 6\sqrt{(b/2b)^2+t^2}-2b$ $Lc = a+2t$
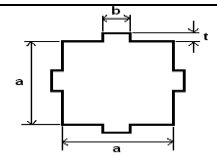	SR-Model $Ac = a^2 + 4(bt)$ $Ap = (a+2t)H$ $P = 4a + 8t$ $Lc = a+2t$	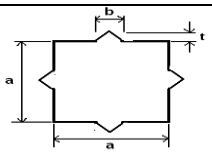	ST-Model $Ac = a^2 + 4(0.5bt)$ $Ap = (a+2t)H$ $P = 4a+ 8\sqrt{(b/2b)^2+t^2}-4b$ $Lc = a+2t$
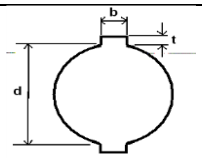	CR-Model $Ac = (\pi/4)d^2 + 2(bt)$ $Ap = dH$ $P = \pi l+ 4t$ $Lc = d+2t$	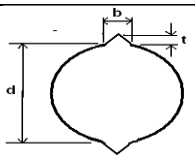	CT-Model $Ac = (\pi/4)d^2+ 2(0.5bt)$ $Ap = dH$ $P = \pi l + 4\sqrt{(b/2b)^2+t^2}-2b$ $Lc = d+2t$
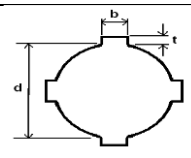	CR-Model $Ac = (\pi/4)d^2 + 4(bt)$ $Ap = (d+2t)H$ $P = \pi l+ 8t$ $Lc = d+2t$	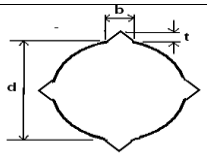	CT-Model $Ac = (\pi/4)d^2+ 4(0.5bt)$ $Ap = (d+4t)H$ $P = \pi l + 8\sqrt{(b/2b)^2+t^2}-4b$ $Lc = d+2t$
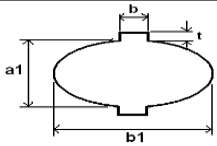	ER-Model $Ac = \pi a_1b_1+ 2(at)$ $Ap = b_1H$ $P = 4a1E(e)+ 4t$ $Lc = b_1$	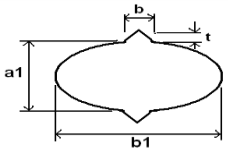	ET-Model $Ac = \pi a_1b_1+ 2(0.2bt)$ $Ap = b1H$ $P =$ $4a1E(e)+ 4\sqrt{(b/2b)^2+t^2}-$

			2b Lc=b1
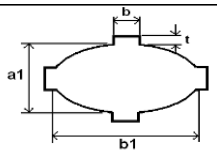	ER-Model Ac = $\pi a_1 b_1$+ 4(at) Ap =(a1+2t)H P = 4a1E(e)+ 8t Lc=b_1+2t	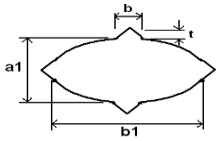	ET-Model Ac = $\pi a_1 b_1$+ 4(0.2bt) Ap ==(a1+4t)H P = 4a1E(e)+ 8$\sqrt{(b/2b)^2+t^2}$-4b Lc=b1+2t

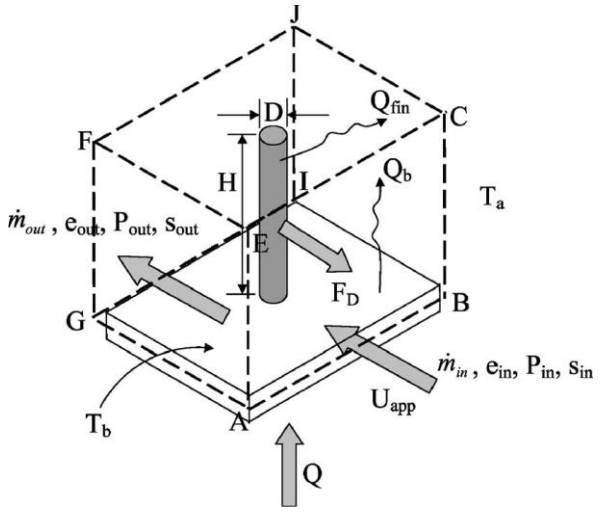

Figure 1. Control volume single circular pin**, Khan** and **Culham, 2003**.

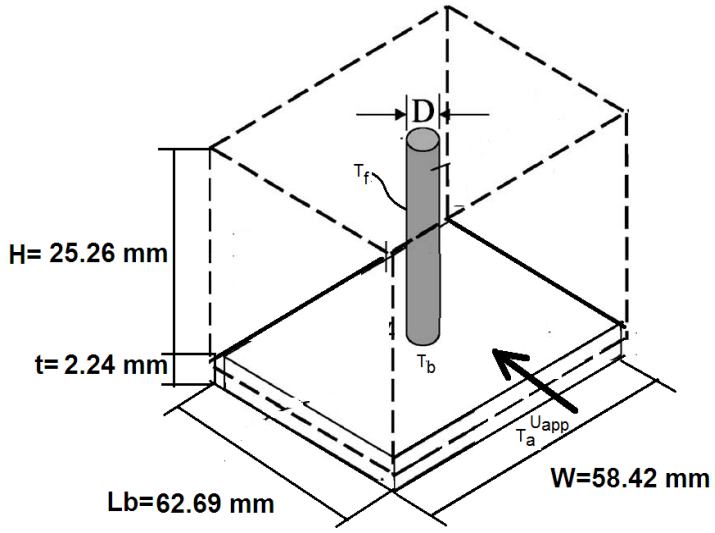

Figure 2. Dimensions and boundary conditions of the base plate and pin fin used in this study.

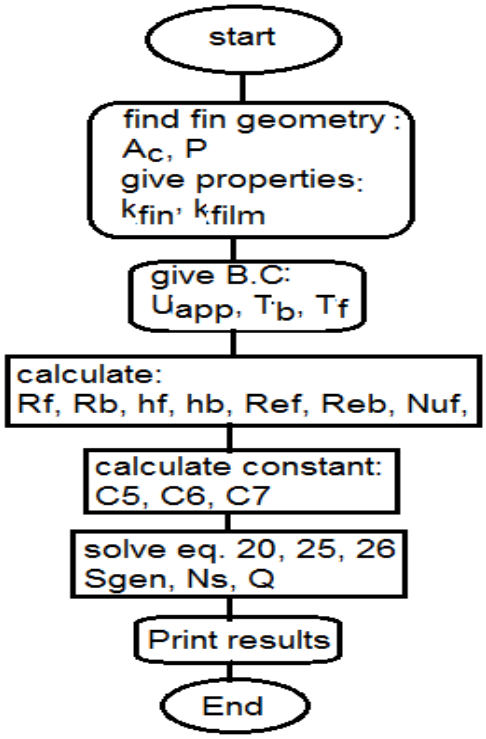

Figure 3. Solution procedure flow chart.

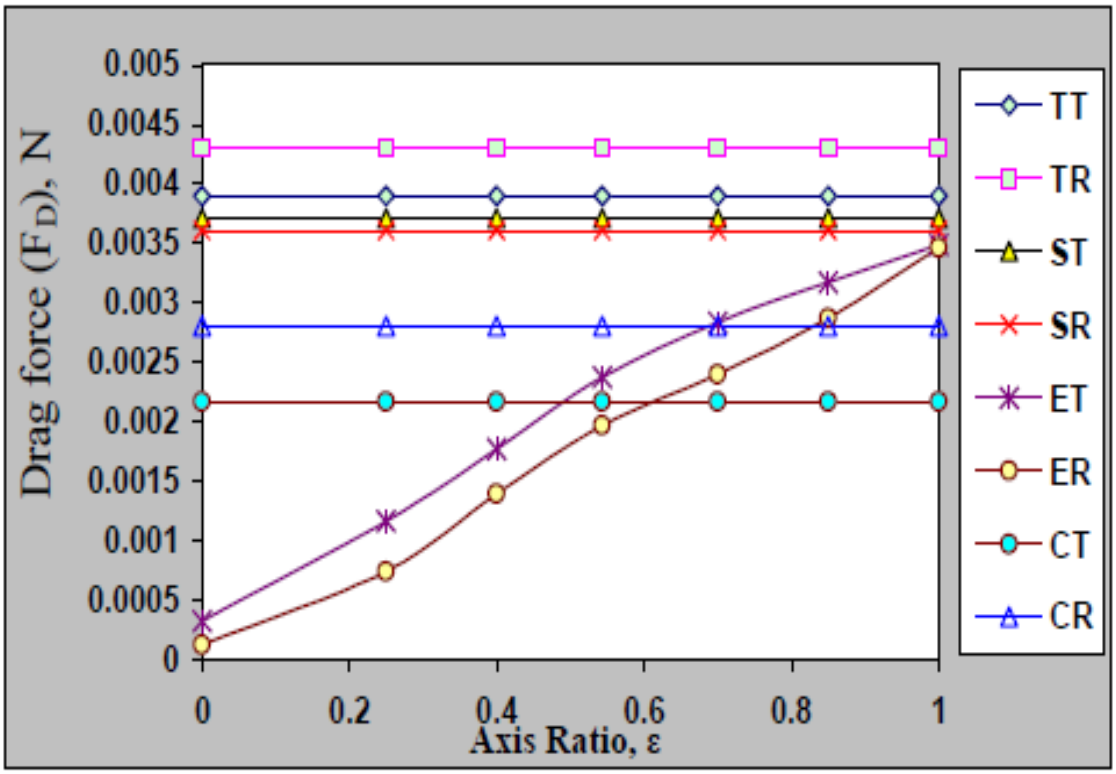

Figure 4. The effect of the axis ratio and the two extra fin of rectangular and triangular on the drag force for all models of cross-sections fins.

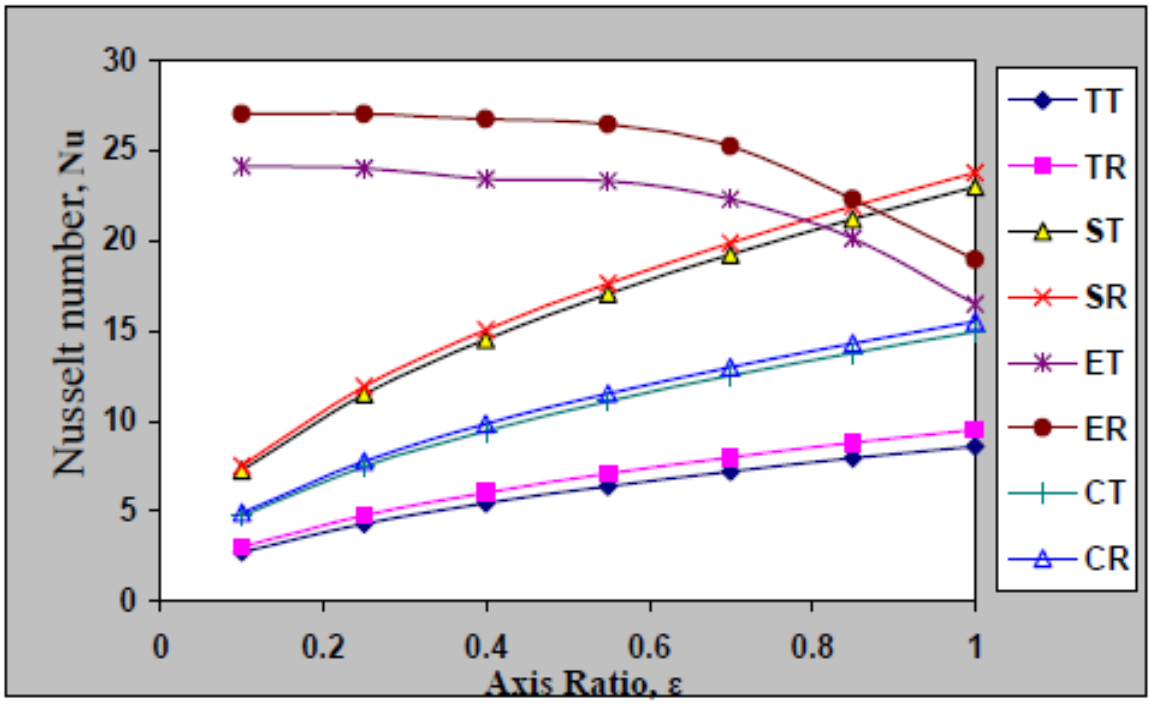

Figure 5. The effect of the axis ratio and the two extra fin of rectangular and triangular on the Nusselt number for all models of cross-sections fins.

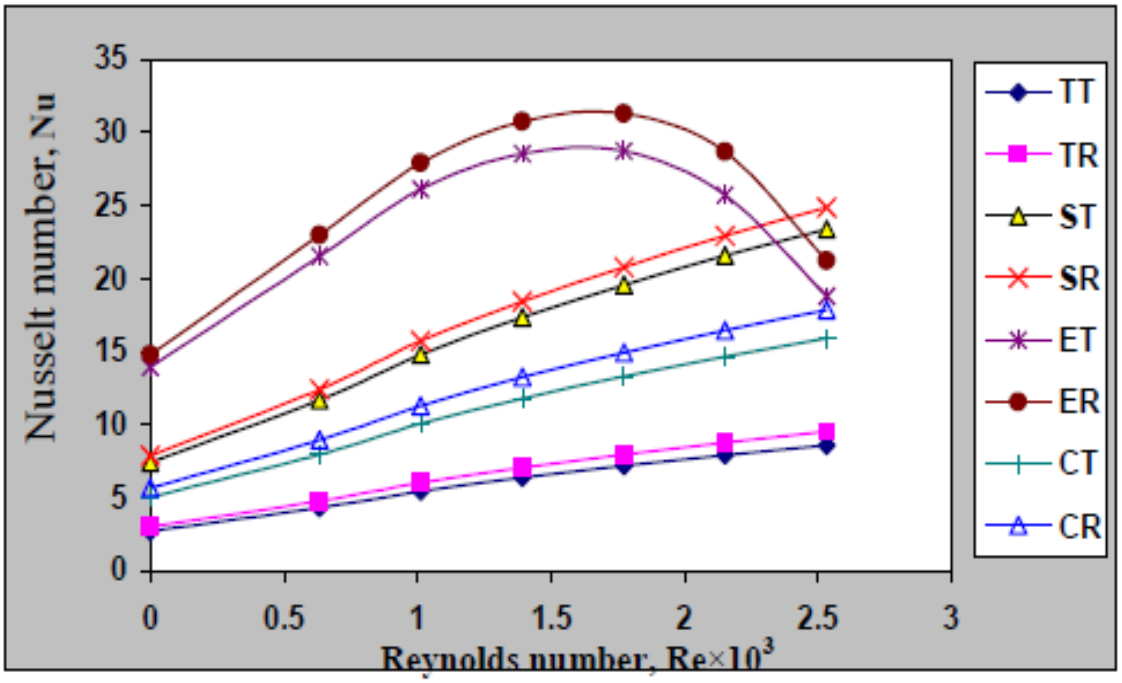

Figure 6. The effect of the Reynolds number based on the characteristic length of the fin and the four extra fin of rectangular and triangular on the Nusselt number for all models of cross-sections fins.

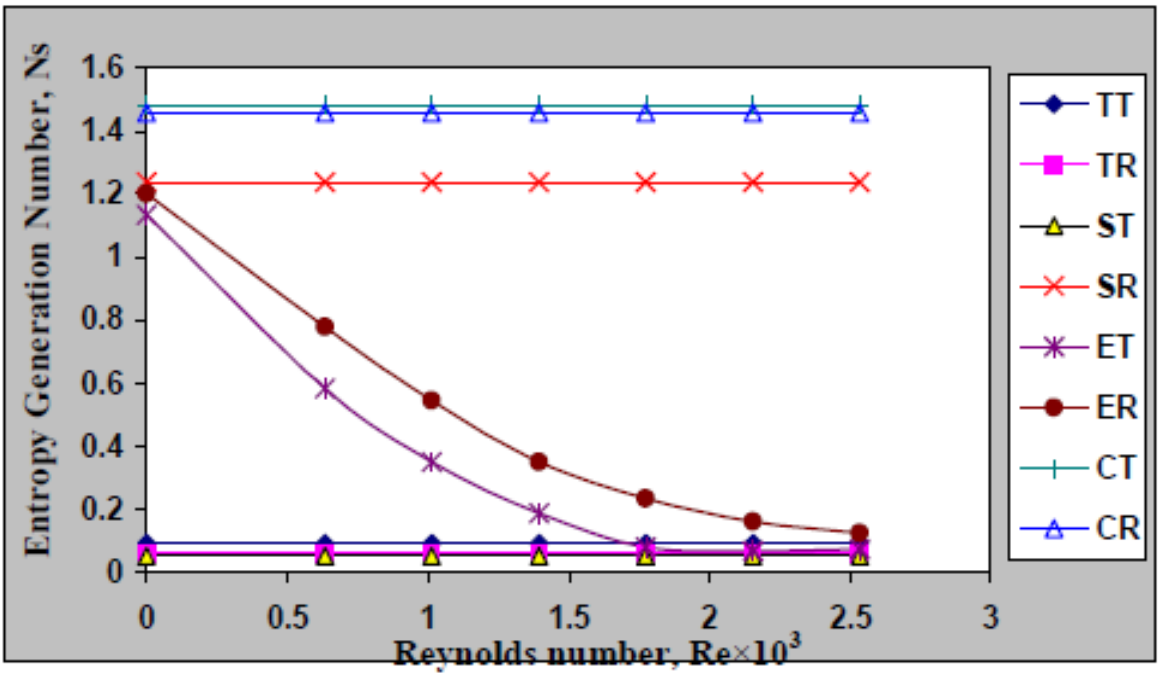

Figure 7. The effect of the Reynolds number and the two extra fin of rectangular and triangular on the dimensionless entropy generation rates for all models of cross-sections fins.

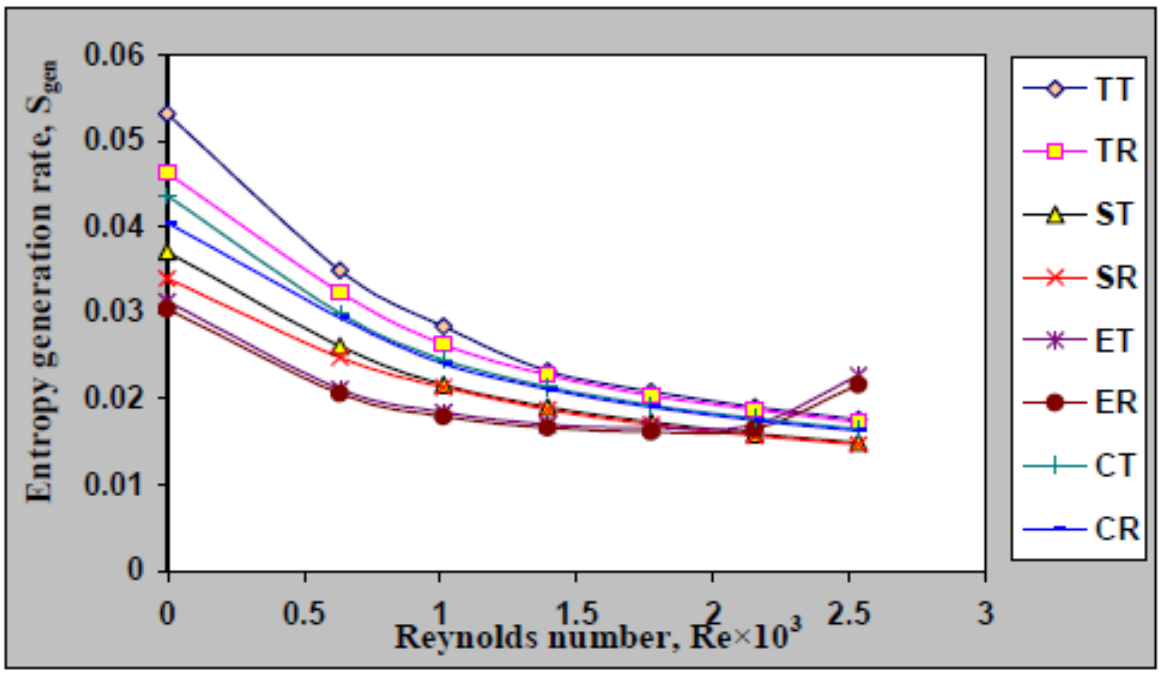

Figure 8. The effect of the Reynolds and the two extra fin of rectangular and triangular on the Dimensionless Entropy Generation Rates for all models of cross-sections fins.

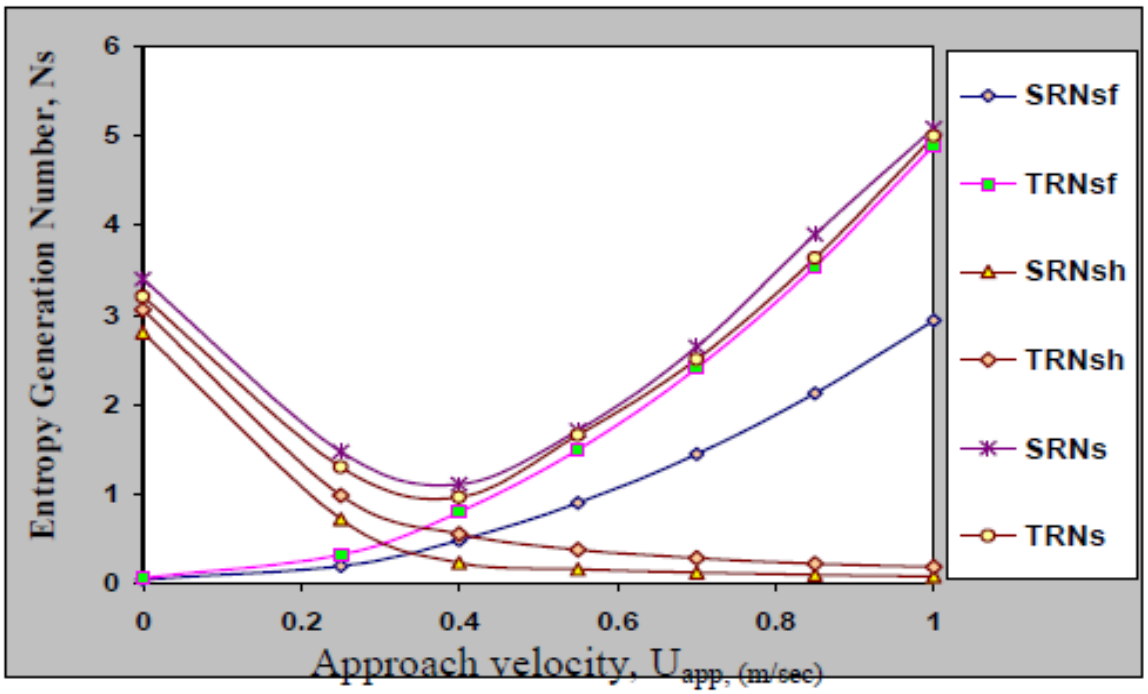

Figure 9. Effect of approach velocity on the dimensionless entropy generation rates for the square and triangular fin geometry with rectangular extra fins.

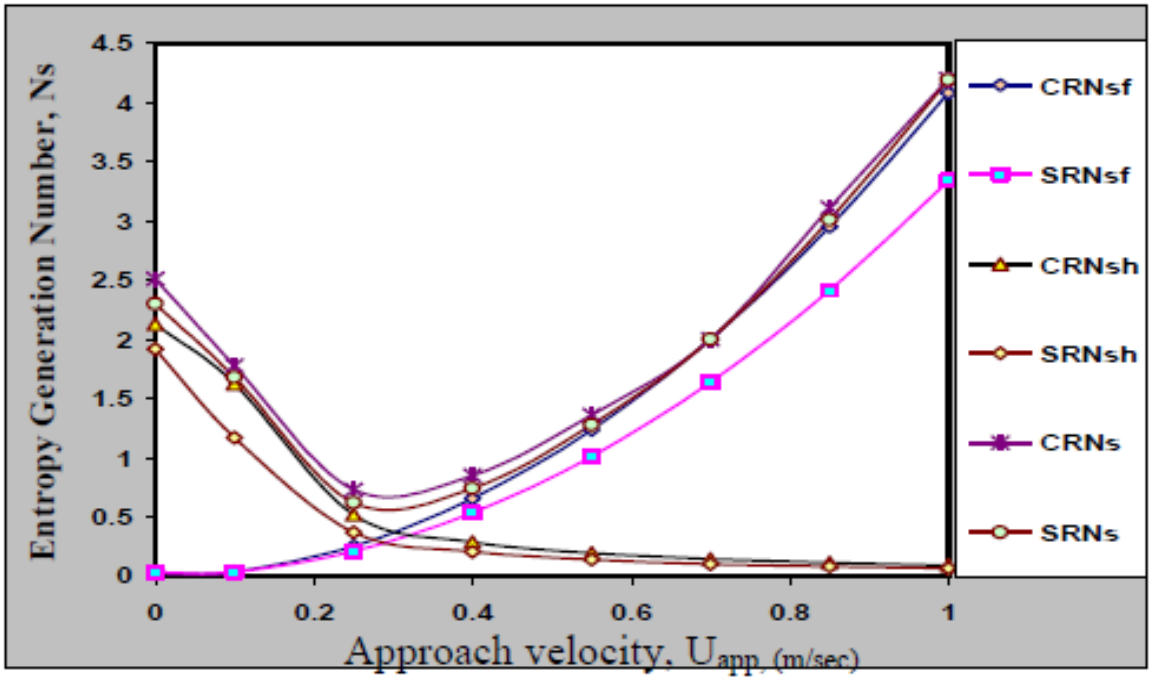

Figure 10. Effect of approach velocity on the dimensionless entropy generation rates for the circular and square fin geometry with rectangular extra fins.

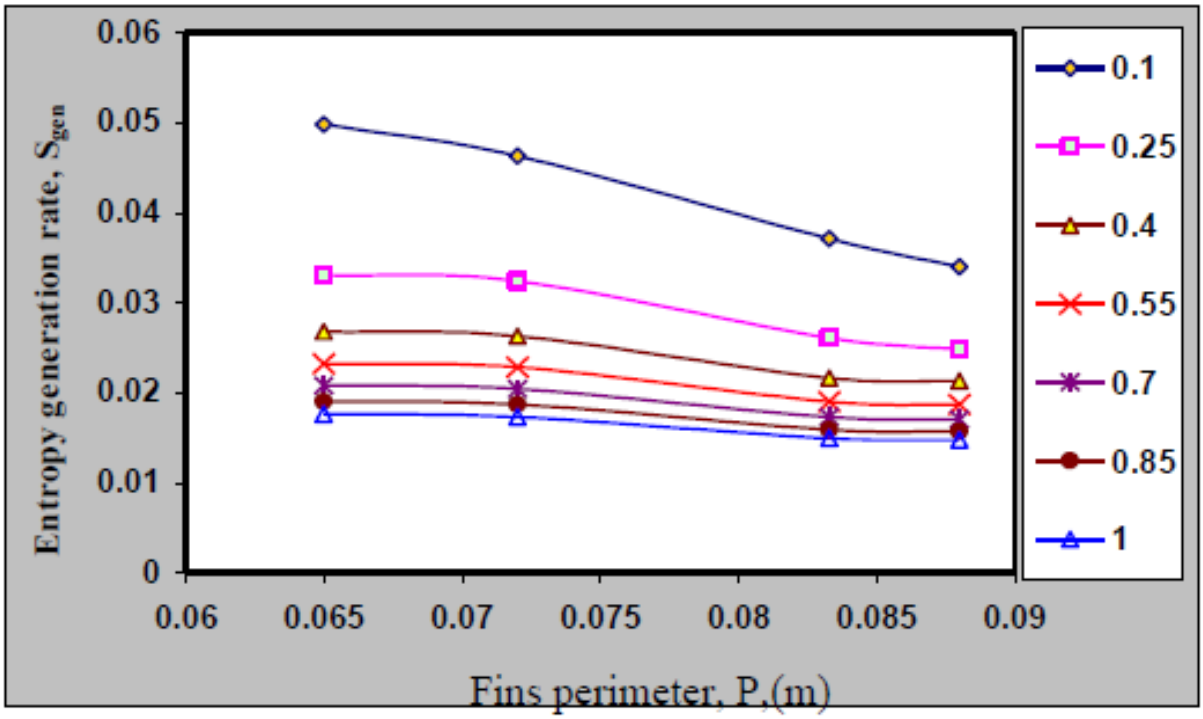

Figure 11. Effect of perimeter on the dimensionless entropy generation rates for all models of fin geometry with rectangular extra fins.

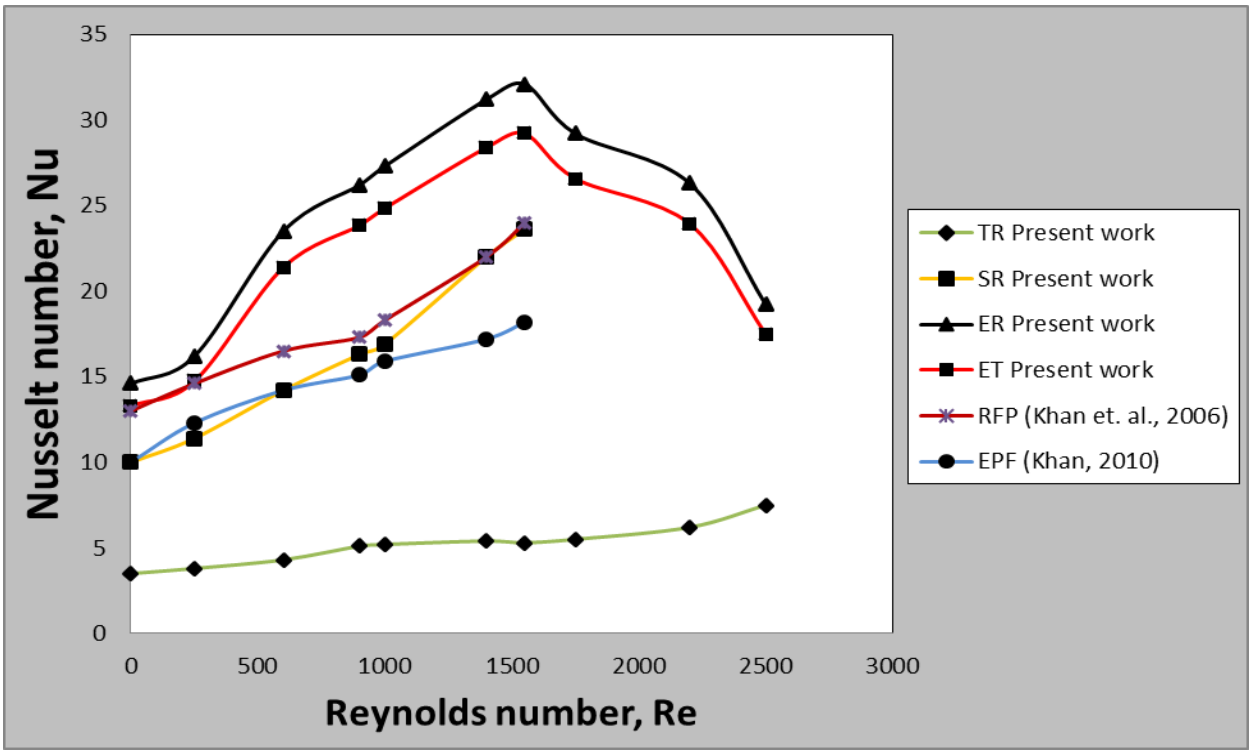

Figure 12. The enhancement of the Nusselt number by comparing the analytical results of the present study with that data studied by **Khan et. al., 2007** and **Khan, 2010**.